# A new analytical generalization of the J and G-theta integrals for planar cracks in a three-dimensional medium

Soliman El Kabir, Frédéric Dubois, Rostand Moutou Pitti, Naman Recho, Yuri Lapusta

# A new analytical generalization of the J and G-theta integrals for planar cracks in a three-dimensional medium

Soliman El Kabir[1], · Frédéric Dubois[1], · Rostand Moutou Pitti[2,4], Naman Recho[2,5], Yuri Lapusta[3]

[1]*University of Limoges, GC2D, EA 3178, Civil Engineering Center, 19300, Egletons, France*

[2]*Université Clermont Auvergne, CNRS, Institut Pascal, F-63000 Clermont Ferrand, France*

[3]*University of Clermont Auvergne, SIGMA Clermont (ex- IFMA), Pascal Institut, BP 10448, F-63000 Clermont Ferrand, France*

[4]*CENAREST, IRT, BP 14070, Libreville, Gabon*

[5]*EPF School of engineering, Sceaux, France*

Corresponding author: Rostand MOUTOU PITTI

Phone: (+33) 4 73 40 75 32 Fax: (+33) 4 73 40 75 10

e-mail: rostand.moutou_pitti@uca.fr

**Abstract** This paper focuses on the theoretical and numerical development of the J-integral concept for three-dimensional problems. A new integral parameter, developed for the real three-dimensional case, computes the combined energy release rate for an arbitrary crack front. A path-independent integral is verified in both the static and crack propagation cases. Generalization of the $J^{3D}$-integral toward its $G_\theta^{3D}$ implementation form is performed. The efficiency of this proposed integral is then compared with a number of $J$ integrals available in the literature. Lastly, the paper offers a finite element implementation along with its numerical validation.

***Keywords:*** *Invariant integral, Linear fracture mechanics, Three-dimensional problems, Energy release rate.*

# Nomenclature

| | |
|---|---|
| $J$ | Rice's integral |
| $J^{3D}$ | three dimensional $J$-integral |
| $\vec{\theta}$ | vector field |
| $G_\theta^{3D}$ | three dimensional $J$-integral with $\vec{\theta}$ fields |
| $(x_1, x_2, x_3)$ | coordinates in a Cartesian reference system |
| $W$ | strain energy density |
| $u, \varepsilon_{ij}, \sigma_{ij}$ | displacements, strains, and stresses components |
| $S$ | surface integral domain |
| $V$ | volume integral domain |
| $n$ | normal vector |
| $S_{out}, S_{in}$ | external and internal surface of the cylinder |
| $S_{cr}-$ and $S_{cr}+$ | lower and upper crack lip surfaces |
| $V_{out}, V_{in}$ | external and internal volume of the cylinder |
| $\Gamma$ | curvilinear integration path |
| $A(\Gamma)$ | area integration path |
| $JA$ | integral proposed by Amestoy *et al.* |
| $\tilde{G}$ | average value of the energy release rate |

| | |
|---|---|
| $P_{j,1}$ | Eshelby's energy-momentum tensor |
| $\delta_{kj}$ | Kronecker symbol |
| $E$ | elastic modulus |
| $\upsilon$ | Poisson's ratio |
| $R_c$ | the inside radius of cylinder |
| $C_w$ | crack width |
| $G(M)$ | energy release rate around a point M |
| $dw$ | strip of width |
| $c_p$ | crown position |

# 1. Introduction

In the field of fracture mechanics and in accordance with global approaches, the energy release rate is usually calculated nowadays using the J-integral [1-2-3] and its derived forms in conjunction with a finite element implementation. The basic J-integral definition assumes that calculations are conducted along a contour around the crack tip in a two-dimensional case. A number of applications have been proposed within many scientific settings for elastic [4], hyperelastic [5], composite [6] and viscoelastic materials [7], generalized to accommodate a crack growth model [8]. The J-integral concept has now been generalized for complex loadings with coupling friction effects [9], transverse loadings [10], mixed-mode configurations [11-12], and fatigue applications [13].

The effects of climatic conditions on the environment are also studied [14-15]. In association with works proposed regarding experimental approaches using J-integrals and digital image correlation techniques as applied to wood, steel and composite materials [16-17-18], all these efforts are limited to a two-dimensional scope [19-20-21-22]. Thin steel or glass composites are some of the materials for which 2D approaches may suffice. However, all studies that account for environmental effects inducing temperature or humidity gradients in the element stiffness require introducing out of-plane effects, such as e.g. torsion (mode III). This reality is more present in thicker structures (e.g. concrete elements, timber structures). A body of work has been undertaken to adapt the J-integral to specific three-dimensional cases [23-24] by means of adding a second integral that incorporates out of-plane stresses [25]. According to the general case, while the J-integral formulation can rather easily be derived in its 2D form, its finite element implementation remains difficult due to the surface integration definition and the necessity to perform interpolations between mesh nodes and integration points. To overcome these hurdles, some authors have suggested various approaches, including the equivalent domain integral [26] and the virtual crack growth method using specific elements near the crack front line [27-28]. This paper therefore discusses the implementation of a generalized J-integral method for three-dimensional media. Ensuring accurate results requires a refined mesh around the crack front line plus the use of specific elements that minimize errors in the interpolation subroutines. In 2D cases, an alternative method allows restricting the interpolation process by transforming the linear integral into a surface integral [29]; this method is called the "theta method" and is capable of respecting the independent path property. These approaches have been proposed for both two-dimensional and axisymmetric problems [30]. This paper is thus focused on generalizing the J-integral formalism for a three-dimensional problem and adapting the G-theta method for future finite element

implementation by considering a three-dimensional problem that includes any crack front and any external loading direction.

As demonstrated on occasion, Noether's approach [31] initiates the development for a three-dimensional medium. The first part of this paper will be devoted to defining a new $J$-integral parameter adapted to three-dimensional problems; it is called the $J^{3D}$-integral, and its definition is used to determine the energy release rate distribution calculated along the crack front line. A generalization of the theta method will be provided in Section 3, along with a presentation of the new $G_\theta^{3D}$-integral, offering a different view of the role of $\vec{\theta}$ distribution along the integration domain and serving to calculate the average energy release rate and its specific value at each point positioned in the crack front line. The last section will compare these global formulations with other authors' formulations. This paper is concluded by a numerical validation section that proves the lack of path dependence within the integration domain and moreover highlights the capacity to calculate the energy release rate distribution along the crack front line in accordance with various shapes. This validation step exposes the distinction between a three-dimensional approach and the typical two-dimensional J-integral.

# 2. Description of the $J^{3D}$-integral

Crack front parameters, which are expressed as a surface integral of stress, strain and displacement derivative terms around a finite-sized path surrounding a crack front, have generally been used as linear and nonlinear fracture parameters. Let's consider a crack front line in a three-dimensional medium, within a Cartesian coordinate system $(x_1, x_2, x_3)$, as a line formed by the intersection of two crack surfaces [32] (see Fig. 1).

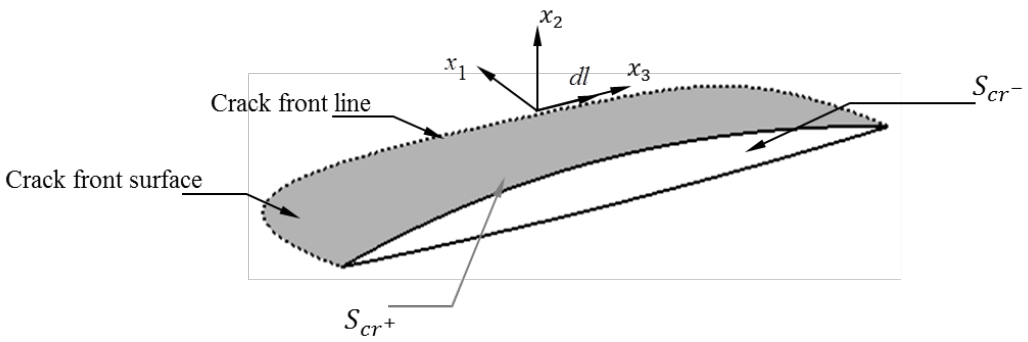


Fig. 1: Crack surface with a crack system coordinate system

The J-integral formulation is based on application of Noether's theorem [31], whereby the strain energy density $W$ is defined by:

$$W(x_1, x_2, x_3) = \int_0^{\varepsilon_{ij}(x_1,x_2,x_3)} \sigma_{ij} d\varepsilon_{ij} \ , (i,j) \in \{1;2;3\}^2 \tag{1}$$

In (1), $(x_1, x_2, x_3)$ denote the coordinates in a Cartesian reference system. The transformed Noether's theorem is based on a stationary Lagrangian condition [33-34-35]; in considering an infinitesimal variation $dW$, Noether's theorem assumes a Lagrangian non-variation. Following the same procedure as that described in [35], a Gauss-Ostrogradski transformation allows expressing the Lagrangian's invariance in the form:

$$\int_S \left(W.n_1 - \left(\sigma_{ij}.n_j.u_{i,1}\right)\right).dS - \int_V \left(W_{,1} - \sigma_{ij}.\left(\varepsilon_{ij}\right)_{,1}\right).dV = 0 \quad (2)$$

where $S$ designates the surface integral domain, oriented by the normal vector $n$, thus delimiting the range of certain assumptions considered in the two-dimensional case [8]. As shown in Figure 2, the integral domain assumes the form of a torus surrounding the crack front line; this form can be considered as the difference between an external volume of the cylinder, $V_{out}$, and the internal volume of the cylinder, $V_{in}$, such that:

$$\boldsymbol{V = V_{out} - V_{in}} \quad (3)$$

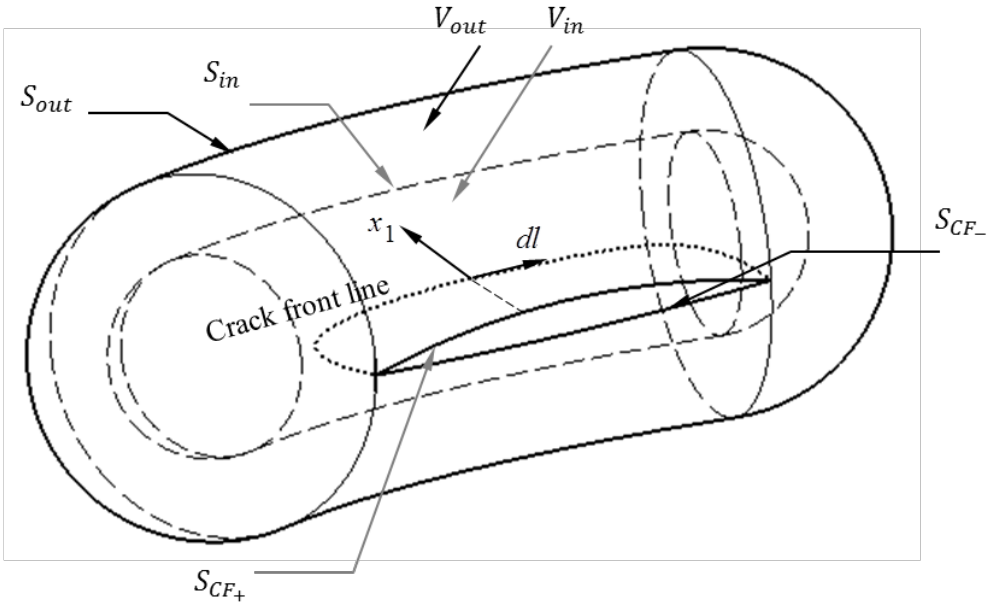


Fig. 2 : Closed volume and surface integration domains

The surface domain is composed of the outside surfaces of $V_{out}$ and $V_{in}$, called respectively $S_{out}$ and $S_{in}$, as well as the lower and upper crack lip surfaces, respectively $S_{cr}-$ and $S_{cr}+$, i.e.:

$$S = (S_{out} + S_{CF_+}) - (S_{in} + S_{CF\_}) \quad (4)$$

Let's note that the minus sign is in accordance with the oriented curvilinear line in a classical two-dimensional problem. In order to simplify the following analytical developments, we have introduced $I_1$ and $I_2$, such that:

$$I_1 = W.n_1 - \left(\sigma_{ij}.n_j.u_{i,1}\right) \; and \; I_2 = \sigma_{ij}.\left(\varepsilon_{ij}\right)_{,1} - W_{,1} \quad (5)$$

In this case, Equation (2) can be written as:

$$\int_S I_1.dS + \int_V I_2.dV = 0 \quad (6)$$

By introducing the surface and volume separations in (4), Equation (6) becomes:

$$\int_{S_{\text{out}}} I_1.dS + \int_{S_{CF_+}} I_1.dS + \int_{V_{\text{out}}} I_2.dV = \int_{S_{\text{in}}} I_1.dS + \int_{S_{CF\_}} I_1.dS + \int_{V_{in}} I_2.dV \quad (7)$$

In considering virtual crack growth in the direction given by the crack orientation and assuming that the crack lips run parallel to the crack growth direction $x_k$, then the component $n_k$ equals zero on the crack lips:

$$\int_{(S_{CF_+})+(S_{CF_-})} I_1.dS = -\int_{(S_{CF_+})+(S_{CF_-})} \sigma_{ij}.n_j.u_{i,k}.dS \tag{8}$$

Moreover, for a surface $S_{in}$ close to the crack front, the volume $V_{in}$ is reduced and tends to zero. We can write:

$$\lim_{\Gamma_{in}\to 0}\left(\int_{V_{in}} I_2.dV\right) = 0 \tag{9}$$

Under such considerations, Equation (7) is reduced as follows:

$$\int_{S_{\text{out}}} I_1.dS + \int_{(S_{CF_+})+(S_{CF_-})} I_1.dS + \int_{V_{\text{out}}} I_2.dV = \lim_{\Gamma_{in}\to 0}\left(\int_{S_{\text{in}}} I_1.dS\right) \tag{10}$$

By analogy with Rice's integral definition in a two-dimensional configuration [3], the right-hand term of (10) designates the *J*-integral, which today is called the $J^{3D}$-integral, as defined below:

$$J^{3D} = \lim_{\Gamma_{in}\to 0}\left(\int_{S_{\text{in}}} I_1.dS\right) \tag{11}$$

We can now write:

$$J^{3D} = \int_{S_{\text{out}}} I_1.dS + \int_{(S_{CF_+})+(S_{CF_-})} I_1.dS + \int_{V_{\text{out}}} I_2.dV \tag{12}$$

Considering Equations (8) and (12) and using the expressions in (5) for $I_1$ and $I_2$, we obtain:

$$\begin{aligned} J^{3D} = \int_{S_{\text{out}}} \left(W.n_k - \left(\sigma_{ij}.n_j.u_{i,k}\right)\right).dS - \int_{(S_{CF_+})+(S_{CF_-})} \sigma_{ij}.n_j.u_{i,k}.dS \\ + \int_{V_{\text{out}}} \left(\sigma_{ij}.\left(\varepsilon_{ij}\right)_{,k} - W_{,k}\right).dV \end{aligned} \tag{13}$$

According to Equation (13), the $J^{3D}$-integral is composed of three separate terms. The first one corresponds to the classical part used to determine crack growth initiation. This term can be completed by the effects of a crack lip pressure introduced by the second term. The last term allows generalizing the crack propagation by ensuring path independence once the crack tip moves inside the integral domain.

# 3. Physical interpretation

This section discusses the physical interpretation of generalizing the J-integral to the $J^{3D}$ integral. Let's consider a crack crossing a plate structure, as shown in Fig. 3. Earlier, Amestoy *et al.* [27] had proposed an initial generalization of the standard *J*-integral to a three-dimensional case by means of writing $J^{3D}$ as:

$$J^{3D} = JA = \int_{\Gamma} \left(W.n_1 - \left(\sigma_{ij}.n_j.u_{i,1}\right)\right).d\Gamma - \int_{A(\Gamma)} \frac{d}{dx_3}\left(\sigma_{i3}.u_{i,1}\right).dA(\Gamma) \tag{14}$$

This definition assumes that the crack lips are oriented in the $x_1$ direction with a linear crack front line parallel to $x_3$. As shown in the expression in (14), the standard J-integral is completed by a second term that integrates the stress components projected into the third dimension. As indicated in Figure 3 however, this form is merely the superposition of a two-dimensional multilayer problem in which the curvilinear integration domain is the intersection between a cylinder, whose generatrix is oriented along $x_3$, and the plane of coordinates $x_3 = 0$ [3].

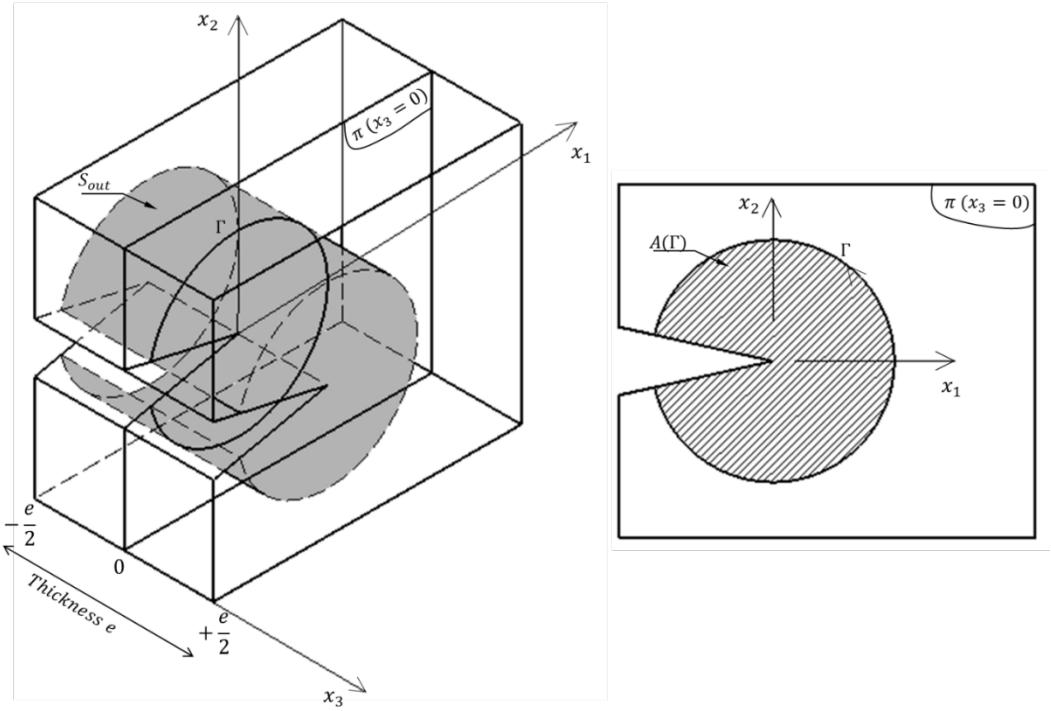


Fig. 3: Surface integration domains for Amestoy's integral

Integrating (14) along the geometry thickness (i.e. along $x_3$) yields:

$$\int_{x_3=-e/2}^{x_3=+e/2} JA.\,dx_3 = \int_{x_3=-e/2}^{x_3=+e/2} \int_{\Gamma} \left(W.n_1 - \left(\sigma_{ij}.n_j.u_{i,1}\right)\right).d\Gamma\,dx_3 - \int_{x_3=-e/2}^{x_3=+e/2} \int_{A(\Gamma)} \frac{d}{dx_3}\left(\sigma_{i3}.u_{i,1}\right).dx_1dx_2dx_3 \tag{15}$$

The link between line Γ and cylinder surface $S_{out}$ is expressed below:

$$S_{\text{out}} = \int_{x_3=-e/2}^{x_3=+e/2} \int_{\Gamma} d\Gamma\,dx_3 \tag{16}$$

Considering the integration domain change in (16), Expression (15) becomes:

$$\int_{x_3=-e/2}^{x_3=+e/2} JA.\,dx_3 = \int_{S_{\text{out}}} \left(W.n_1 - \left(\sigma_{ij}.n_j.u_{i,1}\right)\right).dS - \int_{\substack{A(\Gamma)\\ x_3=0}} \left(\sigma_{i3}.u_{i,1}\right).dx_1dx_2 \tag{17}$$

Next, comparing Expression (17) with the definition of the $J^{3D}$-integral in (13) and considering a stationary crack along with unloaded crack lips, the following can be written:

$$\int_{x_3=-e/2}^{x_3=+e/2} JA.dx_3 = J^{3D} - \int_{\substack{A(\Gamma)\\ x_3=0}} \left(\sigma_{i3}.u_{i,1}\right).dx_1dx_2 \tag{18}$$

In the crack front vicinity, let's note:

$$J^{3D} = \lim_{A(\Gamma)\to 0}\left(\int_{x_3=-\frac{e}{2}}^{x_3=-\frac{e}{2}} JA.dx_3\right) \tag{19}$$

In this form, $J^{3D}$ is interpreted as the integration of the $JA$-integral along the crack front line. In other words, the expression in (19) can be generalized as:

$$J^{3D} = \lim_{A(\Gamma)\to 0}\left(\int_{cfl} JA.dl\right) \tag{20}$$

In this case, the form of the $J^{3D}$-integral may be used to evaluate the average value of the energy release rate $\tilde{G}$ along the crack front line, such that:

$$\tilde{G} = \frac{J^{3D}}{\int_{cfl} dl} \tag{21}$$

This new integral however is unable to calculate the distribution of the energy release rate along the crack front line, which is a necessary calculation in the definition of non-homogeneous crack propagation in the thickness (e.g. elliptical crack). To overcome this limitation, a theta method will prove to be more appropriate in generalizing this three-dimensional formalism for a definition of the energy release rate distribution along the crack front line.

# 4. The $G_\theta^{3D}$-integral

Generalization of the $J^{3D}$-integral toward its $G_\theta^{3D}$ form is based on a Gauss- Ostrogradski transformation [36]. Let's introduce Eshelby's energy-momentum tensor [37], whose components are defined by:

$$P_{j,1} = W.n_1 - \left(\sigma_{ij}.n_j.u_{i,1}\right) \tag{22}$$

Equation (22) corresponds to the first conservative law defined by Knowles and Sternberg [38]. Now, by introducing (22) into (13), we obtain:

$$J^{3D} = \int_{S_{\text{out}}} P_{j,1}.n_j.dS - \int_{(S_{CF+})+(S_{CF-})} \sigma_{ij}.n_j.u_{i,k}.dS + \int_{V_{\text{out}}} \left(\sigma_{ij}.\left(\varepsilon_{ij}\right)_{,k} - W_{,k}\right).dV \tag{23}$$

The generalized formalism, i.e. (23), for any crack propagation direction requires changing the $P_{j,1}$ definition by means of introducing a vector field $\vec{\theta}$, such that:

$$P_{j,1} = P_{j,k}.\theta_k, k \in \{1,2,3\} \tag{24}$$

with:

$$P_{j,k} = W.\delta_{kj} - \left(\sigma_{ij}.u_{i,k}\right) \tag{25}$$

$\delta_{kj}$ is the Kronecker symbol. In the case of crack extension in the $x_k$ direction, the $\vec{\theta}$ coordinates are fixed, on the surface $S_{out}$, at these following values:

$$\theta_k = \delta_{kj} \tag{26}$$

Based on expression (24), Equation (23) can be rewritten as follows:

$$J^{3D} = -\int_{S_{\text{out}}} P_{j,k}.\theta_k.n_j.dS - \int_{(S_{CF_+})+(S_{CF_-})} \sigma_{ij}.u_{i,k}.n_j.\theta_k.dS - \int_{V_{\text{out}}} \left(W_{,k} - \sigma_{ij}.\left(\varepsilon_{ij}\right)_{,k}\right).\theta_k.dV \tag{27}$$

In considering the non-dependence of the integration domain, the transition between the open surface $S_{\text{out}}$ and the $S$ surface becomes possible, hence Equation (27) becomes:

$$J^{3D} = -\int_{S} P_{j,k}.\theta_k.n_j.dS - \int_{(S_{CF_+})+(S_{CF_-})} \sigma_{ij}.u_{i,k}.n_j.\theta_k.dS - \int_{V_{\text{out}}} \left(W_{,k} - \sigma_{ij}.\left(\varepsilon_{ij}\right)_{,k}\right).\theta_k.dV \tag{28}$$

The Gauss-Ostrogradski transformation allows transitioning between a surface integration and a volume integration $V$, situated between $S_{\Gamma_{out}}$ and $S_{\Gamma_{in}}$, in which the theta field equals zero. When applied to the first term in (27), this transformation yields:

$$G_\theta^{3D} = -\int_{V} \left(P_{j,k}.\theta_k\right)_{,j}.dV - \int_{(S_{CF_+})+(S_{CF_-})} \sigma_{ij}.u_{i,k}.n_j.\theta_k.dS - \int_{V_{\text{out}}} \left(W_{,k} - \sigma_{ij}.\left(\varepsilon_{ij}\right)_{,k}\right).\theta_k.dV \tag{29}$$

From Figure 2, the following can be derived:

$$V_{\text{out}} = V_{\text{in}} - V \tag{30}$$

Replacing $V_{\text{out}}$ in Equation (29) leads to:

$$G_\theta^{3D} = -\int_{V} \left(P_{j,k}.\theta_k\right)_{,j}.dV - \int_{(S_{CF_+})+(S_{CF_-})} \sigma_{ij}.u_{i,k}.n_j.\theta_k.dS + \int_{V} \left(W_{,k} - \sigma_{ij}.\left(\varepsilon_{ij}\right)_{,k}\right).\theta_k.dV - \int_{V_{\text{in}}} \left(W_{,k} - \sigma_{ij}.\left(\varepsilon_{ij}\right)_{,k}\right).\theta_k.dV \tag{31}$$

By transforming the derivation in the first integral, Equation (31) is replaced by:

$$G_\theta^{3D} = -\int_{V} \left(P_{kj,j}.\theta_k + P_{kj}.\theta_{k,j}\right).dV - \int_{(S_{CF_+})+(S_{CF_-})} \sigma_{ij}.u_{i,k}.n_j.\theta_k.dS + \int_{V} \left(W_{,k} - \sigma_{ij}.\left(\varepsilon_{ij}\right)_{,k}\right).\theta_k.dV - \int_{V_{\text{in}}} \left(W_{,k} - \sigma_{ij}.\left(\varepsilon_{ij}\right)_{,k}\right).\theta_k.dV \tag{32}$$

In recalling Noether's theorem, as cited in Equation (2), we finally obtain:

$$G_\theta^{3D} = -\int_{V} \left(W.\theta_{k,k} - \left(\sigma_{ij}.u_{i,k}\right).\theta_{k,j}\right).dV - \int_{(S_{CF_+})+(S_{CF_-})} \sigma_{ij}.u_{i,k}.n_j.\theta_k.dS - \int_{V_{\text{in}}} \left(W_{,k} - \sigma_{ij}.\left(\varepsilon_{ij}\right)_{,k}\right).\theta_k.dV \tag{33}$$

The Gauss-Ostrogradski transformation assumes that vector field $\vec{\theta}$ is a vector-derivable function. The form of vector field $\vec{\theta}$ can now be used to obtain different definitions and physical interpretations of this $G_\theta^{3D}$-integral. Let's provide three main applications herein.

a) Average energy release rate value for a rectilinear crack front

As previously shown for the $J^{3D}$-integral, the average value of the energy release rate can be calculated by choosing a specific format for $\vec{\theta}$. Let's consider a rectilinear crack oriented by a constant vector $\vec{c}$ along the sample thickness with a width of $C_w$ (see Fig. 4). The average energy release rate $\tilde{G}$ is calculated using Expression (33) by setting $\vec{\theta}$ to be constant along the width sample, i.e. as follows:

$$\vec{\theta} = \frac{\vec{c}}{|\vec{c}|} \; on \; S_{out} \; and \; \vec{\theta} = 0 \; on \; S_{in} \tag{34}$$

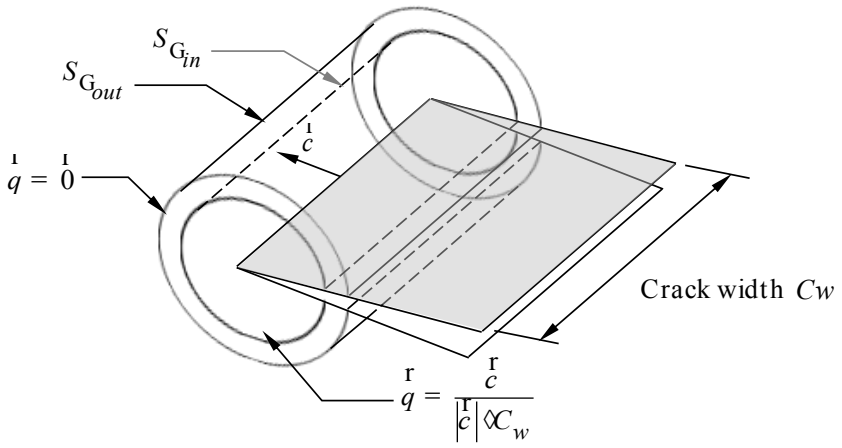


Fig. 4: Crack annotations for a rectilinear crack front

In this case, the $G_\theta^{3D}$-integral is a direct application of the $J^{3D}$-integral. According to the expression in (21), the average energy release rate value is given by:

$$\tilde{G} = \frac{G_\theta^{3D}}{C_\omega} \tag{35}$$

b) Average energy release rate value for a curvilinear crack front

Let's now consider a curvilinear crack oriented along $\vec{c}$ that is assumed to be constant along the crack front (Fig. 5).

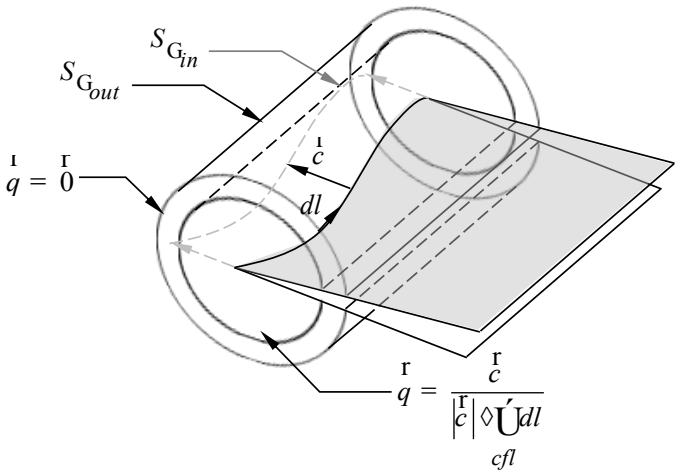


Fig. 5: Crack annotations for a curvilinear crack front

The average energy release rate $\tilde{G}$ is calculated using an analogy with the Expression (34), by substituting the following form for $\vec{\theta}$ (with $cfl$ being the developed crack front width):

$$\vec{\theta} = \frac{\vec{c}}{|\vec{c}|} \; on \; S_{out} \; and \; \vec{\theta} = 0 \; on \; S_{in} \tag{36}$$

c) Energy release rate at a single point

The goal of this calculation is to determine the energy release rate $G(M)$ around a point M, i.e. at any point lying on the crack front. For this application, let's consider a strip of width $dw$, as displayed in Fig. 6. The intersection between this strip and the volume integration domain forms a closed crown $C$, on which the $\vec{\theta}$ field is defined by:

$$\begin{gathered} \vec{\theta} = 0 \; on \; S_{in} \\ \vec{\theta} = 0 \; outside \; the \; close \; crown \\ \vec{\theta} = \frac{\vec{c}}{|\vec{c}|.\, dw} \; on \; C \cap S_{out} \end{gathered} \tag{37}$$

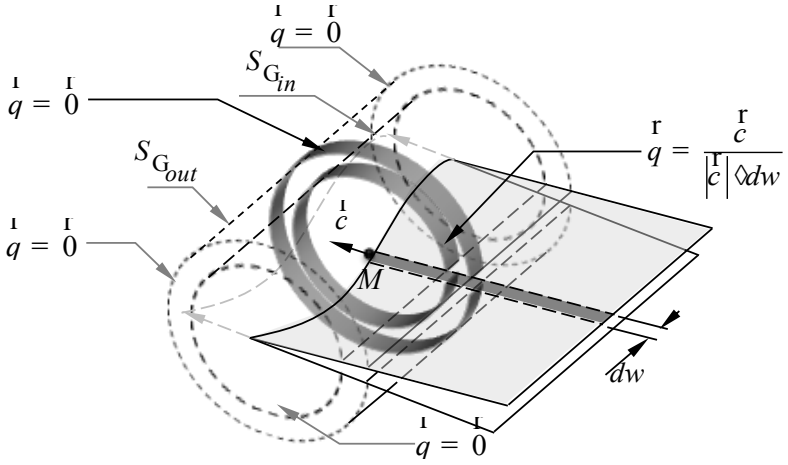


Fig. 6: Definition of $\vec{\theta}$ in the vicinity of a closed crown

The average energy release rate can then be calculated by integrating $G(M)$ along the crack front line divided by the crack width. In this case, at position $l_1$ on the crack front line, the comparison between this $G_\theta^{3D}$-integral and the $J_{Bui}^{3D}$ can be written as follows:

$$J_{Bui}^{3D} = G_\theta^{3D}(\omega) \tag{38}$$

This last application most certainly represents the most significant advance offered by this paper, making it possible to compute the evolution in energy release rate along the crack front. The curvilinear crack front is targeted first, followed by integration of the non-homogeneous energy release distribution induced by the three-dimensional mechanical state of the sample geometry in association with surface boundary conditions.

# 5. Numerical validation

The finite element implementation of this set-up is based on a Double Cantilever Beam submitted to opening mode fracture. We use Cast3M finite element software. This geometry of the Double Cantilever Beam is shown in Fig. 7.

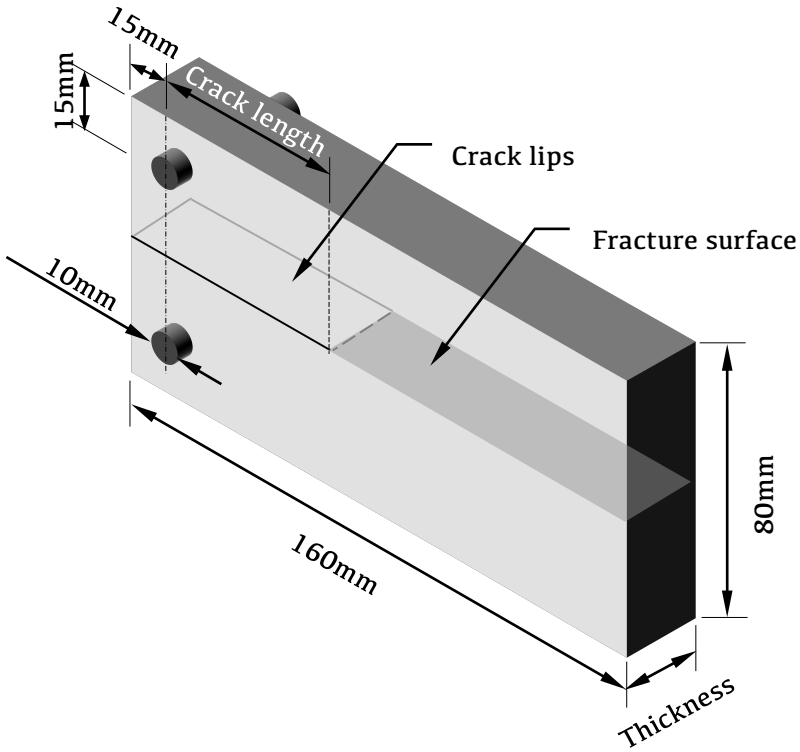


Fig. 7. Double Cantilever Beam geometry

The crack lips and fracture surface reveal a symmetrical surface, thus making it possible to reduce the discretization volume. The displacement loading is applied with the two-hole axes by assuming a frictionless state. In this case, the finite element mesh can assume the shape depicted in Fig. 9, depending on its boundary conditions (Fig. 8).

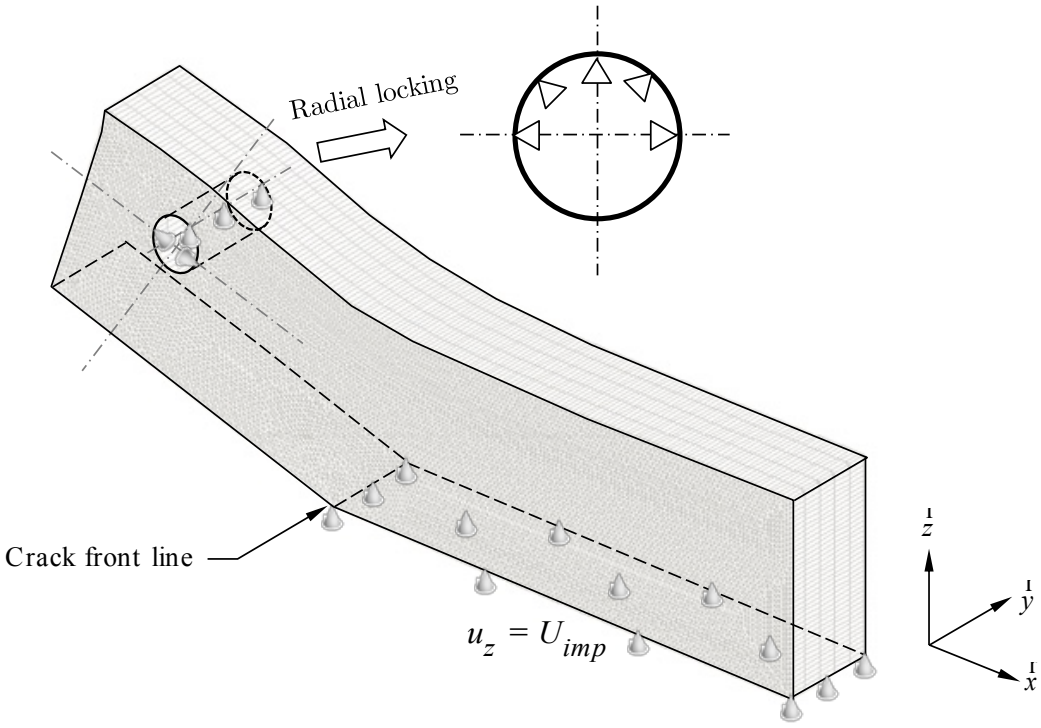


Fig. 8: Boundary conditions

To limit computing time, we have chosen 6-node linear prisms. The loading by imposed displacement is applied at the symmetrical surface and by blocking the hole that models the frictionless contact between the hole axis and the sample. For this theoretical validation step, let's consider an isotropic material, such as steel (mechanical properties: $E = 210GPa$, $\nu = 0.3$). As shown in Fig. 9, the crack front line is surrounded by a cylindrical mesh, inside which the integral domain is defined. The mesh has been divided into two parts.

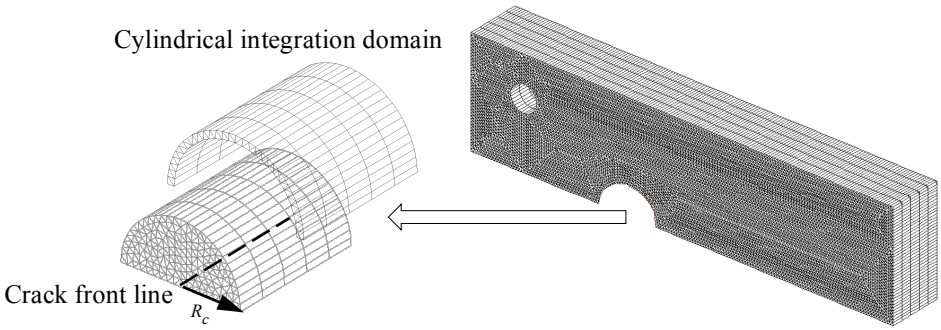


Fig. 9. Integral domain around the crack front line

The first part is a hollow cylinder used to build the theta field using a stationary Fourier's equation, according to which constant temperatures are imposed on both the inside and outside faces. The second part of the mesh is a cylinder surrounded by the crack front line, over which the theta field is a unit constant vector. Let's denote $R_c$ the inside radius of this cylinder. Consider, for example, a straight crack front and a crack extension along $\vec{x}$; consequently, $\vec{\theta}$ and its component $\theta_x$ can be illustrated by Fig. 10.

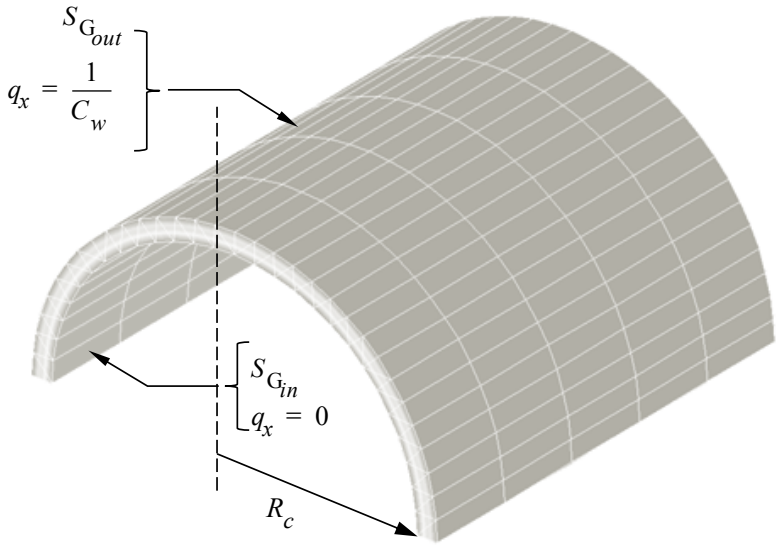


Fig. 10: Component $\boldsymbol{\theta_x}$

Based on this example, the goal of the first application is to validate the non-dependence of the integration domain by varying the size of the integration domain through its radius $R_c$ used to calculate $\overline{G}$. The sample thickness $C_\omega$ is set at 20 mm, and the initial crack length value equals 40 mm. Moreover, we have chosen an imposed displacement of 0.25 mm. As indicated in Fig. 11, the integration domain size has been parameterized with $R_c$ values lying between 1 mm and 22 mm.

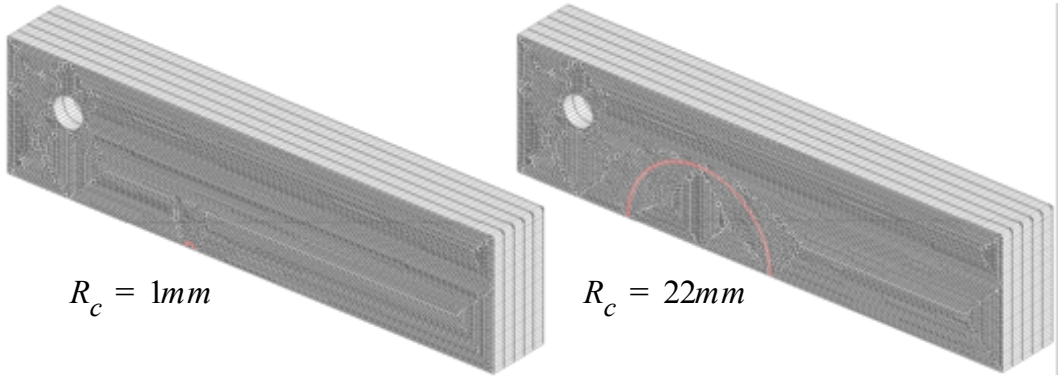


Fig. 11: Integration domain size

Fig. 12 shows the variations in energy release rate vs. $R_c$. Numerical results validate the non-dependence of the integration domain, with an average value of 30.3 kJ/m² and a very small standard deviation (29 J/m²). Note that for $R_c = 1\ mm$, the results display a few artefacts since the mechanical fields present occasional singularities around the crack front.

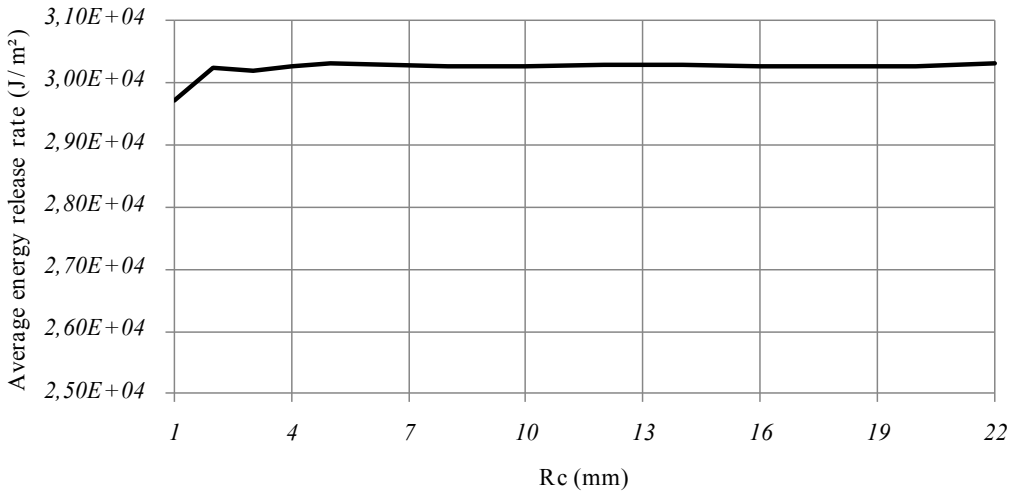


Fig. 12: Average energy release rate vs. Rc

The second validation step entails a comparison with the $JA$-integral proposed by Amestoy *et al.* [25]. In this case, let's focus on calculating the energy release rate at the middle of the crack front line. The main difference consists of how the theta field is defined (see the depiction in Figure 5). In the present case, the theta field is defined on a cylindrical plate domain, as shown in Fig. 13.

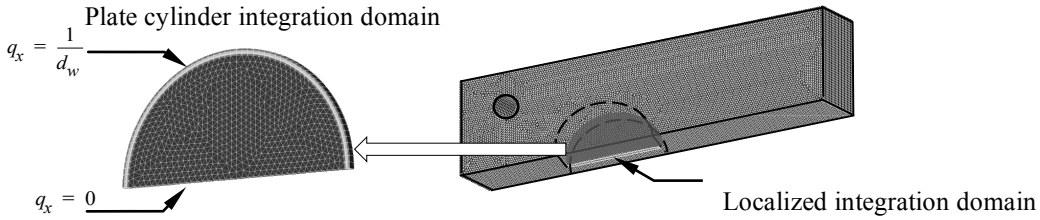


Fig. 13: Integral defined on a cylindrical plate domain around the crack tip

The domain width, labeled $d_\omega$, is localized at a distance $c_p$ (crown position) in a global cylindrical mesh surrounding the crack front line. The average energy release rate is calculated along $d_\omega$. In this first application, the cylinder is considered at the middle of the crack front line, with a 1-mm thickness. In parallel, the $JA$-integral is computed using a 2D configuration, as depicted in Fig. 14, whereby the integration domain is a crown surrounding the crack tip.

The subsequent simulations are intended to compare our 3D approach with the 2D approach generalized by Amestoy [25]; the size of both the 2D and the 3D integration domain is defined using the common radius $R_c$. In the 3D simulation, we have opted for a cylinder centered on the sample stiffness.

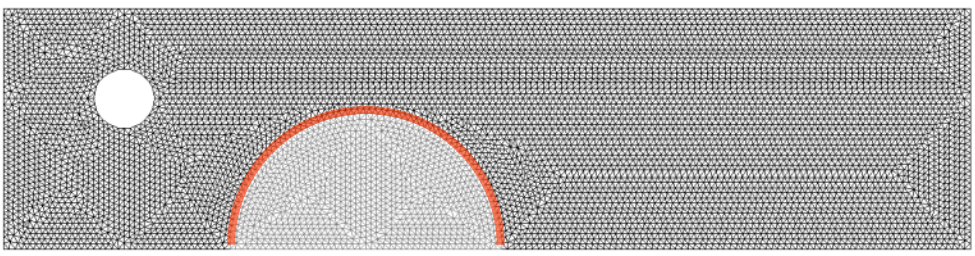

$$R_c = 22mm$$

Fig. 14: Integration domain size for the 2D model

Many simulations are compared in Fig. 15. The reference is the new $J^{3D}$, while $J^{2D}$ represents Rice's classical integral [3], which includes the theta method. Given that the sample thickness appears to be significant with respect to the 2D dimensions (20 mm), we have selected a plane strain configuration. In accordance with the definition of the 3D generalization proposed by Amestoy [25], the additional term in Expression (1) is isolated (i.e. Integral $JA$).

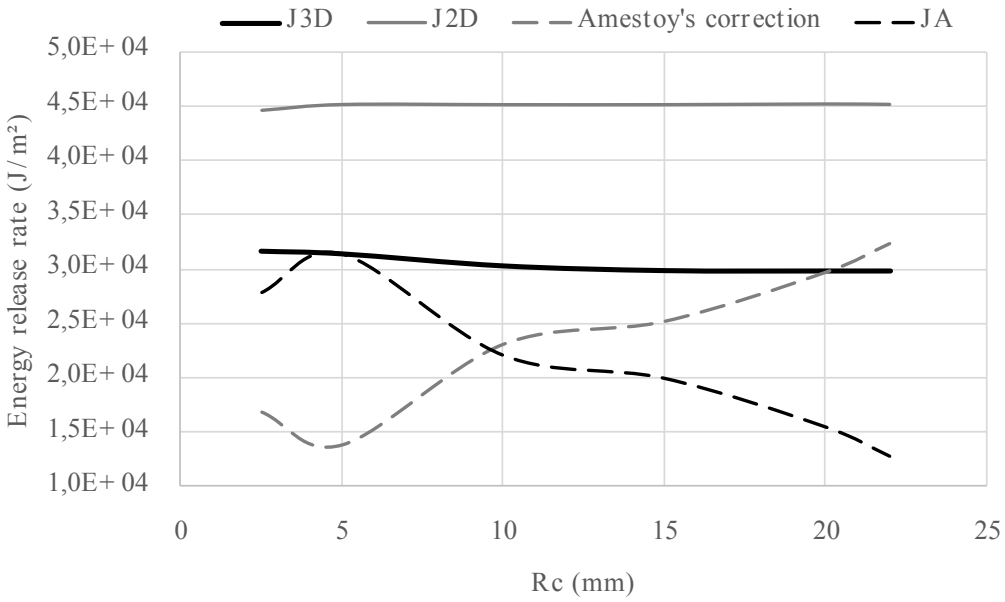


Fig. 15: Comparison between the J2D and J3D approaches

Moreover, Amestoy's integral is denoted $JA$. The results obtained give rise to the following remarks:

- First, the comparison between the classical $J^{2D}$ and $J^{3D}$ highlights a rather sizable discrepancy (greater than 30%) while respecting the non-dependence of integration domains.
- Second, we can reveal the effect of Amestoy's correction on the $J^{2D}$-integral by noting that this additional term does not agree with the non-dependence properties.

With this consideration and in reference to Expression (14), the following equality can be drawn:

$$J^{3D} = J^{2D} - \lim_{A(\Gamma)\to 0} \left| \int_{A(\Gamma)} \frac{\partial}{\partial x_3} (\sigma_{i3}.u_{i,1}) dS \right| \quad (39)$$

Today, the difference between the two- and three-dimensional formulations are consistent with results for stress intensity factors for other mode I geometries [39] and can be explained in several ways. First, the 2D approach must choose either a plane stress or plane strain configuration. Other calculations enable deducing that these two configurations are incapable of explaining such a discrepancy. A second discussion thread focuses on the three-dimensional stress and strain distribution along the crack front. More precisely, they are may be a consequence of corner point singularities [40]. For instance, the Poisson's effect on the crack front could introduce a torsion mode that allows explaining a greater value in terms of energy release rate. Also, the presence of

corner point in the 3D case may contribute to the difference between $J^{2D}$ and $J^{3D}$. Today, we are unable to respond since this investigation requires a separation mode procedure.

The next application considers the evaluation of the energy release rate along the crack front line. According to the integration domain definition shown in Fig. 13 and the non-path dependence property, $R_c$ was set at 20 mm and we opted to calculate the energy release rate distribution along the crack front line by varying $d_\omega$ and $n_\omega$, with a total thickness equal to 20 mm. In this application, the crack front line is always a straight line of finite elements. For each plane cylinder, the energy release rate is calculated at the gravity center projected onto the crack front line. For a discretization of the sample stiffness with $n_\omega = 10$ elements, Fig. 16 indicates the energy release rate distribution along the crack front line vs. thickness.

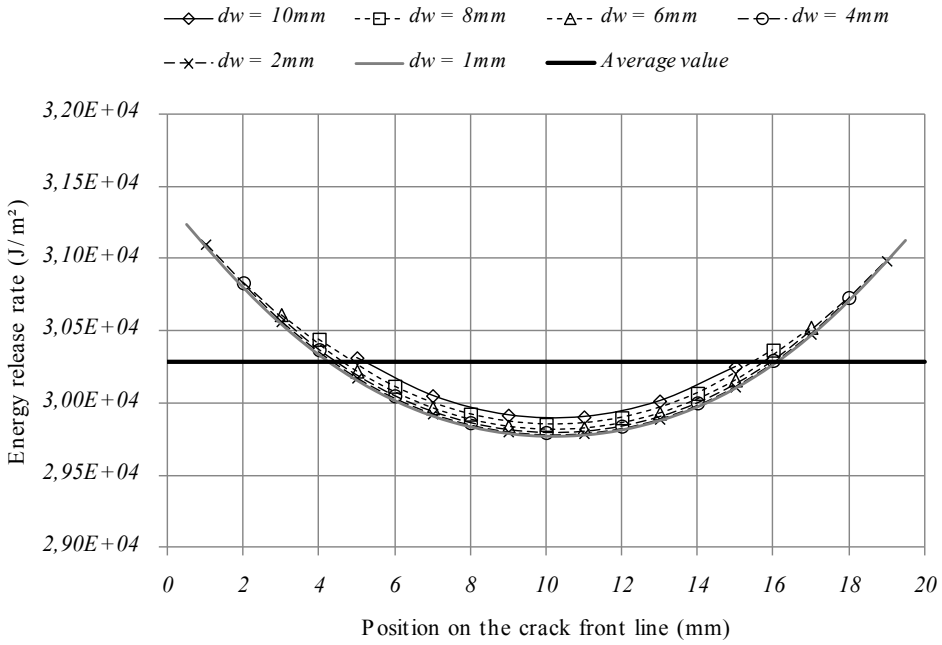


Fig. 16: Energy release rate distribution along the crack front line

This result leads to a few remarks. First of all, the energy release rate distribution exposes a non-heterogeneity of the energy release rate through the sample thickness. Second, this distribution tends to a convergence with a very slim thickness (2 mm in this example). Through this illustration, the figure is completed by means of a calculation that integrates 20 elements along the crack front line plus a 1-mm thickness integration domain (gray line in the figure). Moreover, by comparing average values, equivalent to a 2D configuration, two conclusions can be drawn: the need to take into account the 3D effect on the energy release rate distribution; and during the crack growth process, when considering a crack growth criterion based on a critical energy release rate value, the crack front line must be transformed into a parabolic shape with a longer apparent crack length in the surface than in the sample volume. This approach however requires increased computing power. For example, using an Intel Core i7-4930MX (8 logic processors) and 32 Go of RAM, if the 2D computing is instantaneous, then the time calculation with 20 elements in the thickness sample exceeds 15 minutes with a parallel algorithm solution.

In the vicinity of a corner point, we have a combination between stress intensity factors and corner point singularities. This “double” singular point which is the corner point cannot be represented by any asymptotic analysis. Nevertheless, the corner point can strongly affect the stress field in the

vicinity of the crack tip (see Fig. 17). This last effect is taken into account in our analysis. It's to be noted that once again, if one determines the stress field in order to compute the SIF of corner point that will be influenced by the stress field of the crack tip.

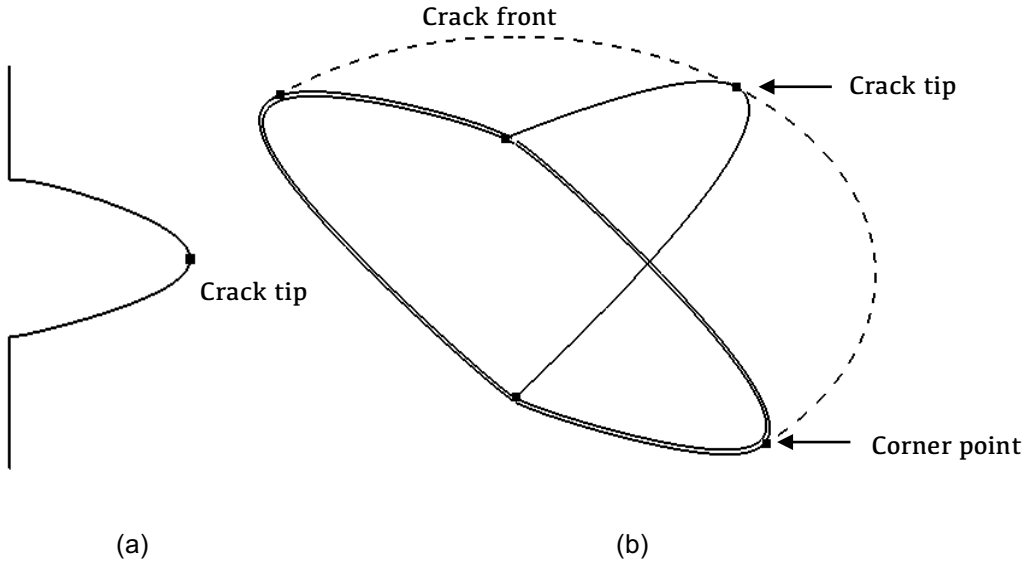


Fig. 17: Illustration of 2D crack tip (a) and corner point in 3D medium (b)

The final application concerns the potential of the $J^{3D}$ in determining the energy release rate distribution for complex crack front line geometry. Based on this same geometry, the mesh near the crack front is deformed in order to obtain a parabolic crack front line (shown in Fig. 18). A total of ten element layers compose the sample stiffness.

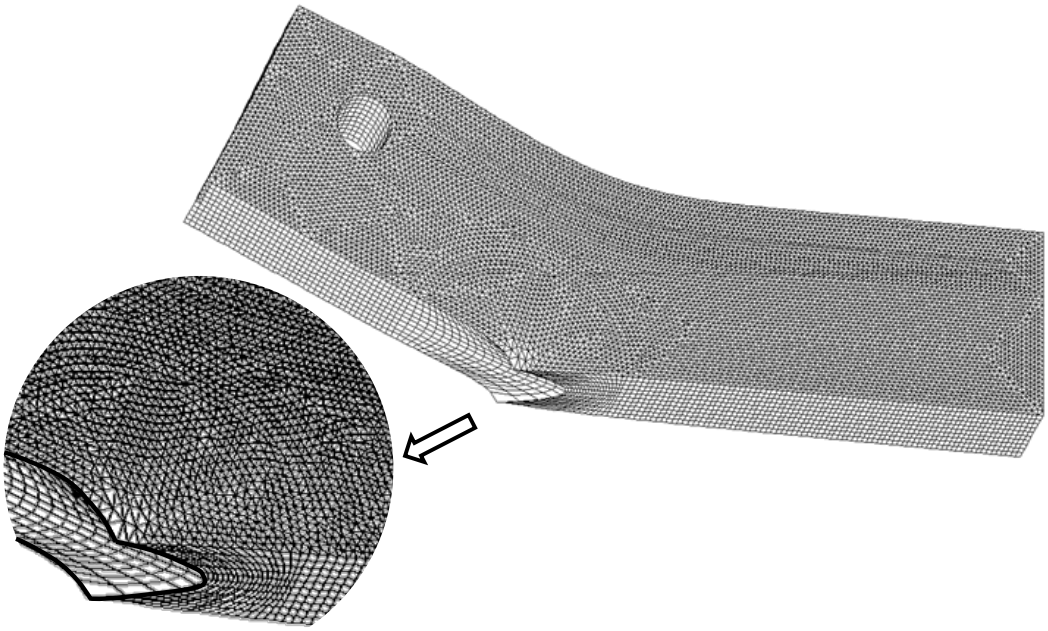


Fig. 18: Finite element mesh containing a parabolic crack front line

According to a two-dimensional vision, the crack length varies between 60 mm at the sample edge and 70 mm at its center. The $J^{2D}$ and Amestoy's form are computed at an equivalent crack length ranging from 61.8 mm to 69.8 mm, corresponding to the barycenter of each element on the sample stiffness. All calculations are performed by assuming a horizontal and axial crack propagation pattern. The full set of results is listed in Table 1. Only the half-specimen has been considered herein. These results reveal a tremendous discrepancy between the two- and three-dimensional approaches induced by the out-of plane-effects, which cannot be integrated into a two-dimensional calculation even with the Amestoy correction.

| Layer | Average crack length (mm) | $J^{3D}$ | $J^{2D}$ | $JA$ |
|---|---|---|---|---|
| 1 | 61.8 | 42394 | 37646 | 30065 |
| 2 | 65 | 21687 | 31710 | 22148 |
| 3 | 67.4 | 14523 | 28034 | 19118 |
| 4 | 69 | 12025 | 25835 | 17417 |
| 5 | 69.8 | 11041 | 24835 | 16673 |

Table 1: Energy release rate output by $J^{3D}$, $J^{2D}$ and Amestoy's integral $JA$ (N/m²)

# 6. Conclusion and outlook

This paper proposes a new formulation of the J-integral for studying the fracture process in elements by considering three-dimensional effects. Compared to a standard two-dimensional computation, this approach includes three-dimensional stress-strain states. Non-path dependence is proven thanks to the use of an analytical formulation. Various visions are proposed in terms of the average energy release rate definition and the energy release rate distribution along the crack front line. Based on a comparison with Amestoy's work, a $G_\theta^{3D}$-integral transformation is proposed for the purpose of computing the energy release rate along the crack front line.

Results of preliminary studies suggest analytic functions of new three-dimensional J-integral useful in numerous applications, including representing of three-dimensional shape of crack front and repartition of energy release rate along this front.

The $J^{3D}$-integral is implemented using the finite element method by considering a theta method. Various developments and validations highlight the capacity of this modeling approach to take into account three-dimensional effects and the out-of-plane stress state. The theta formulation allows defining an average energy release rate or its distribution along the crack front by providing support for the non-dependent integration domain characterizing the invariant integral concept. A comparison with the classical two-dimensional integral highlights the need to consider three-dimensional effects in order to obtain the energy release rate along the crack front. One promising perspective consists of completing this study by a theoretical approach proposing a three-dimensional vision of the local mechanical states in the crack front vicinity, thus offering a relationship between stress intensity factors and the energy release rate and its distribution along the crack front line. This work will serve to introduce virtual mechanical states for extension of the J-integral to a mixed-mode loading case in three-dimensional problems. An M-integral

generalization will allow for a mixed-mode separation with complex geometries and loadings, including tensile, shear and torsion fracture modes.

**Acknowledgments**

The authors would like to express their appreciation to the National Research Agency (ANR) for its financial support of this work through the CLIMBOIS Project No. ANR-13-JS09-0003-01, as certified by the *ViaMeca* organization.

# References

[1] G.R. Irwin. Analysis of stresses and strains near the end of a crack traversing a plate. J Applied Mech, 24 (1957) 361-385.
[2] G.P. Cherepanov. The propagation of cracks in a continuous medium. Journal of Applied Mathematics and Mechanics 31 (1967) 503-512.
[3] JR. Rice. A path independent integral and the approximate analysis of strain conservations by notches and cracks. J. Appl. Mech. 35 (1968) 379–385.
[4] M. Zhang, J. Qu, J.R. Rice. Path independent integrals in equilibrium electro-chemo-elasticity. Journal of the Mechanics and Physics of Solids. 107 (2017) 525–541.
[5] E. Barbieri, F. Ongaro, N.M.A. Pugno. J-integral-based arc-length solver for brittle and ductile crack propagation in finite deformation-finite strain hyperelastic solids with an application to graphene kirigami. Computer Methods in Applied Mechanics and Engineering 315 (2017) 713-743.
[6] N. Serier, B. Mechab, R. Mhamdia, B. Serier. A new formulation of the J integral of bonded composite repair in aircraft structures. Structural Engineering and Mechanics, 58 (5) (2016) 745-755.
[7] F. Dubois, C. Petit. Modelling of the crack growth initiation in viscoelastic media by the $G\theta_v$ −integral. Engineering Fracture Mechanics, 72 (2005) 2821-2836.
[8] F. Dubois, C. Chazal, C. Petit. Viscoelastic crack growth process in wood timbers: an approach by the finite element method for mode I fracture, International Journal of Fracture, 113 (2002) 367–388.
[9] Y.T. Yan, X.-L. Qian, Y.-B. Zhang, Z.-L. Sun. Analysis on crack tip j integral value under sliding contact effect. Journal of Northeastern University, 37(12) (2016) 1744-1749.
[10] X. Fang, P.G. Charalambides. A J-integral approach in characterizing the mechanics of a horizontal crack embedded in a cantilever beam under an end transverse force. Engineering Fracture Mechanics, 169 (2017) 35-53.
[11] R. Moutou Pitti, F. Dubois, O. Pop, J. Absi. A finite element analysis for the mixed mode crack growth in a viscoelastic and orthotropic medium. International Journal of Solids and Structures, 46(20) (2009) 3548-3555.
[12] C. Sarrado, A. Turon, J. Renart, J. Costa. An experimental data reduction method for the Mixed Mode Bending test based on the J-integral approach. Composites Science and Technology, 117 (2015) 85-91.
[13] S. Chapuliot, A. Jaubert, S. Courtin, S. Marie. A ΔJ approach for the evaluation of Fatigue Crack Growth in nozzle corners. International Journal of Pressure Vessels and Piping, 146 (2016) 22-31.
[14] H. Riahi H, R. Moutou Pitti, F. Dubois, A. Chateauneuf. Mixed-mode fracture analysis combining mechanical, thermal and hydrological effects in an isotropic and orthotropic material by means of invariant integrals. Theoretical and Applied Fracture Mechanics 85 (2016) 424-434.
[15] N. Angellier, F. Dubois, R. Moutou Pitti, M. Diakhaté, R.S.A. Loko. Influence of hygrothermal effects in the fracture process in wood under creep loading. Engineering Fracture Mechanics 177 (2017) 153–166.
[16] M. Méité, F. Dubois, O. Pop, J. Absi. Mixed mode fracture properties characterization for wood by Digital Images Correlation and Finite Element Method coupling. Engineering Fracture Mechanics, 105 (2013) 86-100.
[17] G. Catalanotti, P.P. Camanho, J. Xavier, C.G. Dávila, A.T. Marques. Measurement of resistance curves in the longitudinal failure of composites using digital image correlation. Composites Science and Technology, 70 (2010) 1986–1993.

[18] Giancarlo L.G. Gonzáles, Julián A.O. González, Jaime T.P. Castro, José L.F. Freire. A J-integral approach using digital image correlation for evaluating stress intensity factors in fatigue cracks with closure effects. Theoretical and Applied Fracture Mechanics, 90 (2017) 14–21.
[19] R. Moutou Pitti, F. Dubois, C. Petit. Mixed mode fracture separation in viscoelastic orthotropic media: numerical and analytical approach by the Mθv, Int. J. Fract. 145 (2007):181– 193.
[20] R. Moutou Pitti, F. Dubois, C. Petit, N. Sauvat. A new M integral parameter for mixed mode crack growth in orthotropic viscoelastic material. Eng. Fract. Mech. 75 (2008) 4450–4465.
[21] R. Moutou Pitti, F. Dubois, P. Octavian, A proposed mixed-mode fracture for wood under creep loadings. Int. J. Fract. 167 (2) (2011):195-205.
[22] Y.K. Cheung, Y.Z. Chen, New Integral equation for plane elasticity crack problems. Theoretical and Applied Fracture mechanics, 7 (1987) 177-184.
[23] J. Hein, M. Kuna. A generalized J-integral for thermal shock analyses of 3D surface cracks in spatially and temperature dependent materials. Theor. Appled Fract Mech. 2017, https://doi.org/10.1016/j.tafmec.2017.04.013
[24] D. Leguillon. An attempt to extend the 2D coupled criterion for crack nucleation in brittle materials to the 3D case. Theor. Appled Fract Mech. 74 (2014) 7-17.
[25] M. Amestoy, H.D. Bui, R. Labbens, On the definition of local path independent integrals in three dimensional. Mechanics research communications 8(4) (1981) 231-236.
[26] G.P. Nikishkov, S.N. Atluri. Calculation of fracture mechanics parameters for an arbitrary three-dimensional crack, by the equivalent domain integral method. International Journal for Numerical Methods in Engineering, 24 (1987) 1801-1821.
[27] F.Z. Li, C.F. Shih, A. Needleman. A comparison of methods for calculating energy release rates. Engineering Fracture Mechanics, 21 (1985) 405–421.
[28] H.G. Delorenzi. Energy release rate calculations by the finite element method. Engineering Fracture Mechanics, 21(1) (1985) 129-143.
[29] P. Destuynder, P.E.M. Djaoua, L. Chesnay, J.C. Nedelec. Sur une interprétation mathématique de l'intégrale de Rice en théorie de la rupture fragile. Mathematical Methods in the Applied Sciences, 3(1) (1981) 70-87.
[30] F. Dubois, R. Moutou Pitti, B. Picoux, C. Petit. Finite element model for crack growth process in concrete bituminous. Advances in Engineering Software, 44(1) (2012) 35-43.
[31] E. Noether. Invariant variations problems. Trans. Theor. Stat. Phys. 1 (1971) 183–207.
[32] B. Moran, C.F. Shih. Crack tip and associated domain integrals from momentum and energy balance, 27(6) (1987) 615-642.
[33] M. Attigui, C. Petit. Mixed-mode separation in dynamic fracture mechanics: new path independent integrals. Int. J. Fract. 84 (1997) 19–36.
[34] F. Dubois, C. Chazal, C. Petit. Modelling of crack growth initiation in a linear viscoelastic material, J. Theor. Applied Mech. 37 (2) (1999) 207-222.
[35] F. Dubois, C. Chazal, C. Petit. A Finite Element Analysis of Creep-Crack Growth in Viscoelastic Media. Mechanics of Time-Dependent Materials. 2 (1999) 269-286.
[36] R.H. Rigby, M.H. Aliabadi. Decomposition of the mixed-mode J-integral– Revisited. International Journal of Solids and Structures 35 (1998) 2073–2099.
[37] J.D. Eshelby, The Continuum Theory of Lattice Defects, Solid State Physics 3 (1956) 79–144.
[38] J.K. Knowles, E. Sternberg. On a class of conservation laws in linearized and finite elastostatics. 44 (3) (1972) 187-211.
[39] L.P. Pook, A 50- year retrospective review of three-dimensional effects at cracks and sharp notches. Fatigue Fract. Eng. Mater. Struct. 36 (2013) 699-723.
[40] L. P. Pook, F. Berto, A. Campagnolo. State of the art of corner point singularities under in plane and out-of-plane loading. Eng. Fract. Mech. 174 (2017) 2-9.